High-resolution NMR spectroscopy of biological tissues using projected Magic Angle Spinning

Rachel W. Martin[1], Rebecca C. Jachmann[1], Dimitris Sakellariou[2], Ulla Gro Nielsen[3], and Alexander Pines[1]*

[1]Materials Sciences Division, Ernest Orlando Lawrence Berkeley National Laboratory and University of California, Berkeley, CA 94720 USA

[2]Current address: DSM/DRECAM/Service de Chimie Moleculaire, CEA/Saclay, 91191 Gif sur Yvette, France.

[3]Current address: Chemistry Department, SUNY Stony Brook, NY 11794-3400 USA

* Correspondence to: Prof. A. Pines, Department of Chemistry, D64 Hildebrand Hall,
University of California, Berkeley, CA 94720 USA
Tel. (510) 642-1220 Fax (510) 486-5744 pines@berkeley.edu

Abstract:

High-resolution NMR spectra of materials subject to anisotropic broadening are usually obtained by rotating the sample about the magic angle, which is 54.7° to the static magnetic field. In projected Magic Angle Spinning (p-MAS), the sample is spun about two angles, neither of which is the magic angle. This provides a method of obtaining isotropic spectra while spinning at shallow angles. The p-MAS experiment may be used in situations where spinning the sample at the magic angle is not possible due to geometric or other constraints, allowing the choice of spinning angle to be determined by factors such as the shape of the sample, rather than by the spin physics. The application of this technique to bovine tissue samples is demonstrated as a proof of principle for future biological or medical applications.

Keywords: Nuclear Magnetic Resonance, magnetic susceptibility broadening, rotating solids, biological tissue

Introduction:

Proton (^{1}H) NMR studies of metabolites in biological tissue have been extensively used to monitor changes in cellular function as a result of disease, e.g. (1-5). In tissue, resolving signals for the metabolites of interest can be difficult because the lines are often broad and overlapping. The primary mechanism of this broadening is local magnetic field gradients caused by variations in the bulk magnetic susceptibility (6,7). This effect can be alleviated by Magic Angle Spinning (MAS), a technique for averaging anisotropic interactions transforming under spatial motion as the second order Legendre polynomial, $P_2\cos(\theta)$. In MAS (8), the sample is rotated about an axis that makes an angle of $\cos^{-1}\sqrt{1/3} \approx 54.7°$ with respect to the static magnetic field B_0.

High-speed MAS is routinely used in high-resolution solid-state NMR studies of diverse materials such as inorganic solids, polymers, and macromolecular crystals. Several techniques have been developed for obtaining the same type of resolved isotropic spectra at the slower spinning speeds required for fragile samples such as intact organs or even living animals. When the spinning speed is less than the width of the anisotropic spectrum, spinning sidebands appear at multiples of the spinning speed, obscuring the spectrum and lowering the effective signal-to-noise ratio. Sideband suppression by rotor synchronized pulse sequences such as 1D-TOSS (9) and 2D-PASS (10) has been used in slow-spinning studies of excised human tissue (4,11). Magic Angle Hopping (MAH), in which the sample hops between three discrete positions during the pulse sequence (12), and Magic Angle Turning (MAT), its continuous rotation analogue (13-15), are related techniques for acquiring isotropic-anisotropic correlations. MAT spectra of metabolites in tissues and organs have been recently acquired for both excised tissues (16) and a living mouse (17). In these applications, rotor synchronized pulses produce an isotropic spectrum in one dimension and a manifold of sidebands covering the full powder pattern in a second dimension, correlating isotropic and anisotropic information in a two-dimensional NMR experiment. This allows the isotropic spectrum to be recovered without the need for fast spinning, as well as retaining potentially valuable information derived from anisotropic interactions.

The purpose of the p-MAS experiment is to obtain high-resolution two-dimensional spectra containing isotropic and anisotropic spectral information by spinning the sample at two angles, both of which may be much less than the magic angle. This method can produce a scaled isotropic spectrum even in situations where spinning at the magic angle is not feasible. Although the spinning speeds used in this preliminary study are faster than can be tolerated by a living animal, p-MAS could enable high-resolution spectra of elongated samples or intact, although

nonliving, organisms. Hardware and pulse sequences for a slow-spinning extension of p-MAS, named projected Magic Angle Turning (p-MAT), are currently under development. The p-MAT experiment will allow slower off-magic angle spinning; eventually enabling in-vivo NMR studies on live animals. Because p-MAT is technically demanding, the present study was conducted to ascertain whether p-MAS, which was initially demonstrated using model systems, is feasible for reducing anisotropic broadening in tissue samples (18). The results indicate that the observed broadening in tissue samples is spatially correlated as in the model system, providing motivation for the further development of p-MAT.

For a spin system characterized by anisotropic broadening and subjected to sample spinning that is much larger than the relevant interactions, the Hamiltonian can be written as a sum of the isotropic and anisotropic parts.

$$H_0(\theta) = H_{iso} + P_2\cos(\theta)H_{aniso} \quad (1)$$

The p-MAS pulse sequence is shown in figure 1. The experiment consists of evolution for time t_1 at an angle θ_1, after which the signal is detected during t_2 at a second angle θ_2. The magnetization is stored along z during the period τ required for angle switching and stabilization (typically tens of milliseconds). This experiment gives a correlation between two anisotropic dimensions, with the width of the spectrum in each dimension determined by the values of $P_2\cos(\theta)$ for θ_1 and θ_2, respectively. The isotropic information is recovered by a shearing transformation performed along an axis determined by the ratio of the polynomials for the two angles.

To the extent that the residual linewidths do not scale with the angle, the choice of angles used is limited by a chemical shift scaling factor (λ) that depends on the difference between the spinning angles, as well as on the angles themselves:

$$\lambda = \frac{P_2(\cos\theta_1) - P_2(\cos\theta_2)}{P_2(\cos\theta_1) + P_2(\cos\theta_2)} \quad (2)$$

Figure 2 shows a plot of the scaling factor for different pairs of spinning angles, given a constant inherent linewidth that is smaller than the induced broadening. Because the scaling depends on the absolute value of the angles, as well as the difference between them, the scaling can be very small for angles close to zero. This would appear to severely curtail the usefulness of the technique, however as far as the residual linewidth is caused by inhomogeneous interactions that are also scaled by the angle, this is not a problem. In order for the p-MAS experiment to give a useful result, the linewidth produced by the magnetic susceptibility differences must be larger than the linewidth contribution caused by homogeneous broadening mechanisms such as T_2, and the chemical shift difference between the observed resonances must be larger than the effective

scaling induced by the p-MAS experiment. The minimum linewidth of the p-MAS projection depends on the degree to which the distribution of frequencies present is correlated. If the interactions are perfectly correlated, the projected experiment will result in the isotropic spectrum (19). Chemical shift changes due to susceptibility differences or B_0 inhomogeneities are highly correlated, while those induced by sample disorder may not be (20).

In the case of tissue samples, the linewidths are dominated by magnetic susceptibility. Because of the high mobility of small molecules in tissue, residual dipolar couplings are much smaller, on the order of 20 Hz (21). This contribution is easily averaged out at the spinning speeds used here. However, residual dipolar couplings have been observed for metabolites in muscle samples in vivo and used to investigate muscle fiber ordering effects (21,22). This may be an interesting topic for future multidimensional p-MAS experiments correlating isotropic spectra with dipolar coupling information. In this preliminary work, p-MAS is used to investigate the effectiveness of removing anisotropic interactions in biological tissue by spinning a sample at small angles relative to the static field.

Methods:

Samples of bovine muscle and liver were obtained from a supermarket and prepared by soaking for 20 hours in a solution of 0.05 M NaCl in D_2O. Saline solution allows stabilization of the tissue at near-physiological salt concentration while reducing the intensity of the water resonance and those of other exchangeable protons in the sample. Proton exchange was used in lieu of water suppression for these preliminary experiments. Future experiments may include water suppression added to the pulse sequence. The samples were packed into a 4 mm Varian Pencil MAS rotor, using Kel-F spacers fitted with fluorosilicon o-rings on either side of the sample (23) in order to prevent dehydration of the sample during the experiment. This method was found to preserve the spectral resolution of the sample over periods of several days.

Proton NMR spectra were acquired on a Chemagnetics (Varian) Infinity spectrometer operating at 500 MHz ^{1}H Larmor frequency, using an extensively modified Varian 4 mm HX switched angle spinning probe. In order to provide a constant amplitude and phase of the B_1 field independent of the spinning angle, a split solenoid coil was used. A similar coil design was employed in recent switched angle spinning experiments (24). Unlike a traditional solenoid oriented parallel to the spinning axis, this type of coil provides a constant B_1 field directed perpendicular to the B_0 field regardless of the coil's orientation. Because sensitivity was not limiting in these experiments, the resulting loss in B_1 homogeneity was minimized by restricting the sample to a small homogeneous region in the center of the coil.

Static and MAS one-dimensional ^{1}H spectra were collected using a Bloch decay sequence with a B_1 frequency of approximately 50 kHz. Static spectra were collected with an acquisition length of 8192 points and a spectral width of 20 kHz in 16 scans (muscle), and 64 scans (liver). The MAS spectrum of the muscle was collected in 4 scans at a spinning frequency of approximately 1.7 kHz using an acquisition length of 8192 points and a spectral width of 20 kHz. For the liver, the MAS spectrum at 6 kHz spinning speed was collected in 64 scans with an acquisition length of 8192 points and a spectral width of 30 kHz. Chemical shifts were referenced to the ^{1}H resonance of water at 4.7 ppm.

Two-dimensional data sets were collected using the p-MAS pulse sequence (18), which is depicted in figure 1. Phase cycling was used to achieve frequency sign discrimination in both dimensions (25). The angles used in this experiment were $\theta_1 = 4.5°$ and $\theta_2 = 26°$ for both samples. The angle switching/stabilization period (τ) was 50 ms. The precision of the angle setting is estimated to be 0.1 degrees. For the muscle sample, 256 points were collected in the indirect dimension (f1) and 2048 in the direct dimension (f2) at a spectral width of 10 kHz in each dimension. The spinning speed used was approximately 2 kHz. 16 scans were recorded for each point in the indirect dimension. For the liver sample, the same parameters were used, except for the spinning speed, which was approximately 6 kHz. Isotropic spectra were recovered from the 2D data by using a shearing transformation followed by a projection, as described in an earlier publication. The scaling factor for the isotropic chemical shifts depends on the choice of angles (18) and was 0.16 in this case.

Results and Discussion:

Figure 3 shows data collected on bovine muscle. The static spectrum (a) shows strong signals for water and triglyceride methylene protons (4.7 ppm and 1.2 ppm, respectively) along with poorly resolved resonances for other components. Under MAS (b), several more resonances can be clearly observed. Partial assignments based on previously published results (16,26) are presented in the figure caption. The appropriate projection of the p-MAS spectrum (c) after a shearing transformation and adjustment for the scaling imposed on the isotropic chemical shifts by the experiment shows the same information as the MAS spectrum. The 2D p-MAS spectrum is plotted in figure 4 in order to illustrate the type of data that are obtained from this experiment before data processing. In this 2D spectrum, broad lines appear in the direct and indirect dimensions, however shearing the spectrum along an axis determined by the ratio of the two angles used allows reconstruction of the isotropic spectrum. All of the resonances that are assignable in the 1D spectrum are also visible in the projection of the p-MAS spectrum (figure

1c). It should be noted that the residual linewidths observed in the p-MAS projection are slightly greater than in the MAS spectrum. This effect is not due any inherent limitation in the experiment, but to truncation of the time domain signal in the indirect dimension, which is a familiar problem in high-resolution multidimensional NMR experiments. Such effects may be minimized by data prediction using standard methods such as linear prediction or maximum entropy. Because p-MAS is an inherently two-dimensional technique, the experiment time required is longer than for a 1D spectrum, and resolution in the indirect dimension may be time limited. However, the objective is not to replace MAS, but allow experiments to be performed under conditions that would otherwise be impossible, such as in the case of an elongated sample that cannot be spun at the magic angle inside the bore of a magnet.

Figure 5 shows data collected on bovine liver. The static spectrum (a) shows a large water signal at 4.7 ppm and a broad resonance representing the other components of the tissue, but signals from individual metabolites cannot be distinguished. In the MAS spectrum (b) more detailed information is shown. The region between 0-4 ppm (c) contains several distinct resonances corresponding to metabolites, which can be assigned based on earlier work (16,27). Details of these assignments may be found in the figure caption. The projection of the p-MAS spectrum (d) reveals the same resonances as are observed in the MAS spectrum. In the liver sample, the linewidth is approximately the same in the p-MAS projection as in the MAS spectrum, indicating that the indirect FID is not truncated. This is because the resonances in the liver sample have a larger inherent linewidths than those in the muscle, possibly because of the higher concentration of paramagnetic components in this tissue, or because of its morphology.

MAS depends on each spin returning to the same place in space at the end of a rotor period. Molecular diffusion randomizes this and causes decoherence to the extent that it occurs on the timescale of the rotor period as spins diffuse to a different region of the tissue that may represent a different chemical or magnetic local environment. Molecular diffusion is typically not a major source of line broadening in MAS at the spinning speeds used here. For spinning speeds greater than 100 Hz the linewidth contribution from diffusion scales as $\frac{1}{F_r^2}$, where F_r is the rotor frequency in Hz. However, diffusion during the hopping time between the angles will contribute to the linewidth. Minimizing this time is desirable in order to reduce effects from molecular diffusion as well as spin diffusion in the p-MAS experiment.

Conclusions:

For studies of tissue samples, the p-MAS technique produces spectra that are functionally equivalent to conventional MAS spectra. It is possible to use p-MAS to separate resonances for different metabolites from that of water in liver and muscle tissue. This demonstrates the potential utility of p-MAS for less invasive *in vivo* studies of biological tissues, with the possibility of obtaining better quality results by adding water suppression to the p-MAS experiment or by detecting other nuclei exhibiting a larger range of chemical shifts such as ^{13}C or ^{31}P in future experiments. Within the constraints imposed by scaling of the chemical shift, the p-MAS technique allows the choice of spinning angle to be made based on factors such as the sample geometry or the electromagnetic power requirements, rather than as a consequence of the spin physics. This should prove useful in cases where the sample cannot be spun at the magic angle, for instance when the sample is elongated and must be rotated at shallower angles in order to fit inside the magnet bore.

These experiments also serve as a proof of principle for future experiments in which the sample remains static and the field is rotated around it. In the adiabatic limit, spinning the magnetic field is equivalent to spinning the sample (8). In the first experimental implementation of this idea, narrowing of a line broadened by dipolar couplings was observed in a sample of solid hyperpolarized xenon (28). Further improvements of this method are likely to require p-MAS because the power required to rotate a magnetic field increases dramatically as the angle of rotation increases. Thus, if small spinning angles are used, stronger magnetic fields may be rotated. Therefore, small-angle rotation techniques such as p-MAS may be the deciding factor in making it possible to use a magnetic field large enough to obtain the necessary sensitivity and resolution.

Acknowledgments:

RWM acknowledges the Department of the Army, contract DAMD 17-03-1-0476 for support.
UGN acknowledges Carlsbergfondet (ANS-0634/20) for a post-doctoral fellowship.
This work was supported by the Director, Office of Basic Energy Sciences, Materials Science Division of the U.S. Department of Energy under contract number DE-AC03-76SF00098.

References:

1. Bollard ME, Garrod S, Holmes E, Lindon JC, Humpfer E, Spraul M, Nicholson JK. High-resolution ^{1}H and ^{1}H-^{13}C magic angle spinning spectroscopy of rat liver. Magnetic Resonance in Medicine 2000;44:201-207.
2. Ross RD. The biochemistry of living tissues: examination by MRS. Nuclear Magnetic Resonance in Biomedicine 1992;5:303-324.
3. Sitter B, Sonnewald U, Spraul M, Fjosne HE, Gribbestad IS. High-resolution magic angle spinning MRS of breast cancer tissue. NMR in Biomedicine 2002;15:327-337.
4. Taylor JL, Wu CL, Cory D, Gonzales RG, Bielecki A, Cheng LL. High-resolution magic angle spinning proton NMR analysis of human prostate tissue with slow spinning rates. Magnetic Resonance in Medicine 2003;50:627-632.
5. Rooney OM, Troke J, Nicholson JK, Griffin JL. High-resolution diffusion and relaxation-edited magic angle spinning ^{1}H NMR spectroscopy of intact liver tissue. Magnetic Resonance in Medicine 2003;50:925-930.
6. Chen JH, Enloe BM, Xiao Y, Cory DG, Singer S. Isotropic susceptibility shift under MAS: The origin of the split water resonances in ^{1}H MAS NMR spectra of cell suspensions. Magnetic Resonance in Medicine 2003;50:515-521.
7. Adebodun F, Post JFM. Bulk magnetic susceptibility induced line broadening in the ^{19}F spectra of suspended leukemic cells. NMR in Biomedicine 1993;6:125-129.
8. Andrew ER, Bradbury A, Eades RG. Removal of dipolar broadening of nuclear magnetic resonance spectra of solids by specimen rotation. Nature 1959;183:1802-1803.
9. Dixon WT. Spinning-sideband-free and spinning-sideband-only NMR spectra in a spinning sample. Journal of Chemical Physics 1982;77:1800-1809.
10. Antzutkin ON, Shekar SC, Levitt MH. Two-dimensional sideband separation in magic-angle-spinning NMR. Journal of Magnetic Resonance 1995;115A:7-19.
11. Wu CL, Taylor JL, He W, Zepeda AG, Halpern EF, Bielecki A, Gonzales RG, Cheng LL. Proton high-resolution magic angle spinning NMR analysis of fresh and previously frozen tissue of Human prostate. Magnetic Resonance in Medicine 2003;50:1307-1311.
12. Bax A, Szeverenyi NM, Maciel GE. Correlation of isotropic shifts and chemical shift anisotropies by two-dimensional Fourier-transform magic-angle hopping NMR spectroscopy. Journal of Magnetic Resonance 1983;52:147-152.
13. Gan Z. High-resolution chemical shift and chemical shift anisotropy correlation in solids using slow magic angle spinning. Journal of the American Chemical Society 1992;114:8307-8309.
14. Hu JZ, Wang W, Pugmire RJ. Magic angle turning and hopping. In: Grant DM, K. HR, editors. Encyclopedia of Nuclear Magnetic Resonance. New York: Wiley and Sons; 1996. p 2914-2921.
15. Hu JZ, Wind RA. The evaluation of different MAS techniques at low spinning rates in aqueous samples and in the presence of magnetic susceptibility gradients. Journal of Magnetic Resonance 2002;159:92-100.
16. Wind RA, Hu JA, Rommereim DN. High-resolution ^{1}H NMR spectroscopy in organs and tissues using slow magic angle spinning. Magnetic Resonance in Medicine 2001;46:213-218.
17. Wind RA, Hu JZ, Rommereim DM. High-resolution ^{1}H NMR spectroscopy in a live mouse subjected to 1.5 Hz magic angle spinning. Magnetic Resonance in Medicine 2003;50:1113-1119.
18. Sakellariou D, Meriles CA, Martin RW, Pines A. High-resolution NMR of anisotropic samples with spinning away from the magic angle. Chemical Physics Letters 2003;377:333-339.
19. Brown SP, Wimperis S. Inhomogeneous broadening of two-dimensional NMR lineshapes. Chemical Physics Letters 1995;237:509-515.
20. Sakellariou D, Brown SP, Lesage A, Hediger S, Bardet M, Meriles CA, Pines A, Emsley L. High-resolution NMR correlation spectra of disordered solids. Journal of the American Chemical Society 2003;125:4376-4380.
21. Schroder L, Bachert P. Evidence for a dipolar-coupled AM system in carnosine in human calf muscle from in vivo ^{1}H NMR spectroscopy. Journal of Magnetic Resonance 2003;164:256-269.

22. Boesch C, Kreis R. Dipolar coupling and ordering effects observed in magnetic resonance spectra of skeletal muscle. NMR in Biomedicine 2001;14:140-148.
23. Martin RW, Paulson EK, Zilm KW. Design of a triple resonance magic angle sample spinning probe for high field solid state nuclear magnetic resonance. Review of Scientific Instruments 2003;74(6):3045-3061.
24. Havlin RH, Park GHJ, Mazur T, Pines A. Using switched angle spinning to simplify NMR spectra of strongly oriented samples. Journal of the American Chemical Society 2003;125:7998-8006.
25. Mueller KT, Sun BQ, Chingas GC, Zwanziger JW, Terao T, Pines A. Journal of Magnetic Resonance 1990;86:470.
26. Williams SR, Gadian DG, Proctor E, Sprague DB, Talbot DF, Young IR, Brown FF. Proton NMR studies of muscle metabolites *in vivo*. Journal of Magnetic Resonance 1985;63:406-412.
27. Hu JZ. High-resolution ^{1}H NMR spectroscopy in rat liver using magic angle turning at a 1 Hz spinning rate. Magnetic Resonance in Medicine 2002;47:829-836.
28. Meriles CA, Sakellariou D, Moule A, Goldman M, Budinger TF, Pines A. High-resolution NMR of static samples by rotation of the magnetic field. Journal of Magnetic Resonance 2004;169:13-18.

Figures:

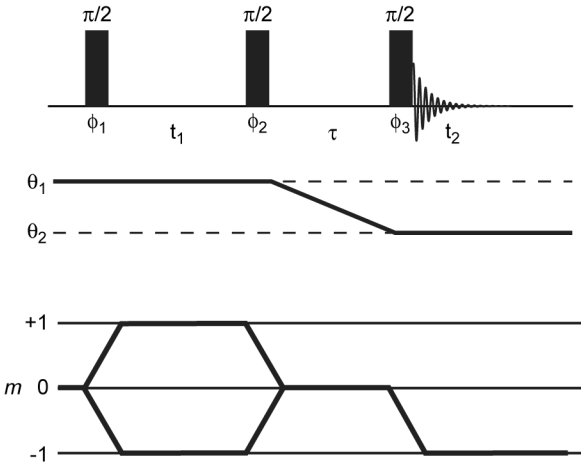

figure 1

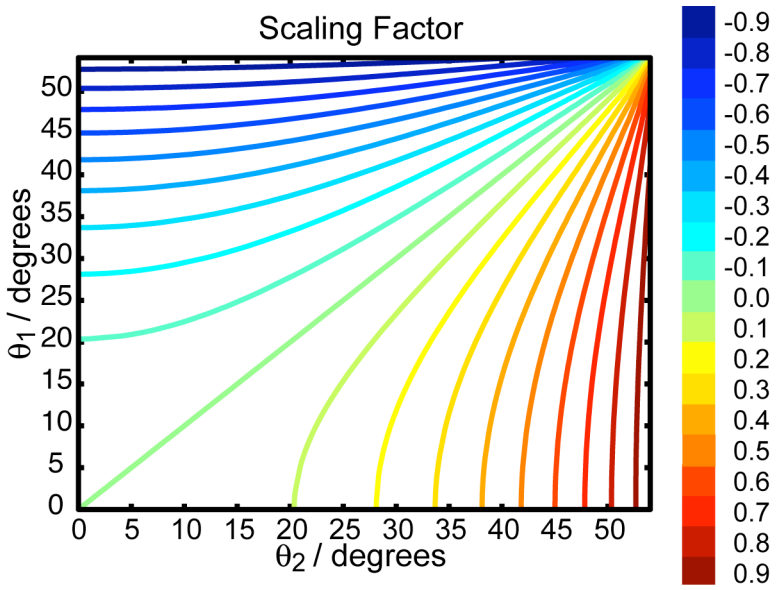
Scaling Factor
θ1 / degrees
θ2 / degrees
0
5
10
15
20
25
30
35
40
45
50
-0.9
-0.8
-0.7
-0.6
-0.5
-0.4
-0.3
-0.2
-0.1
0.0
0.1
0.2
0.3
0.4
0.5
0.6
0.7
0.8
0.9

figure 2

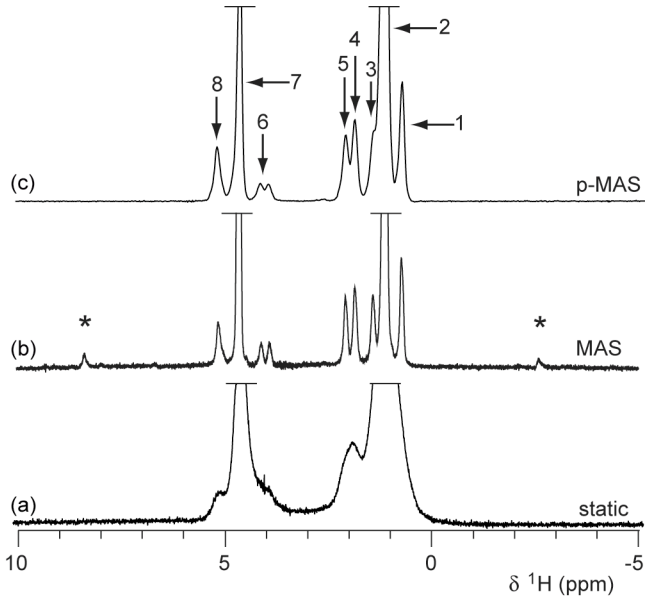

figure 3

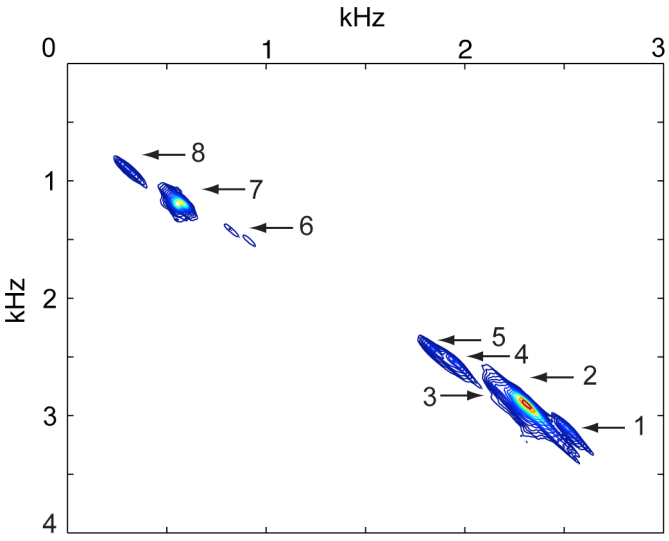

figure 4

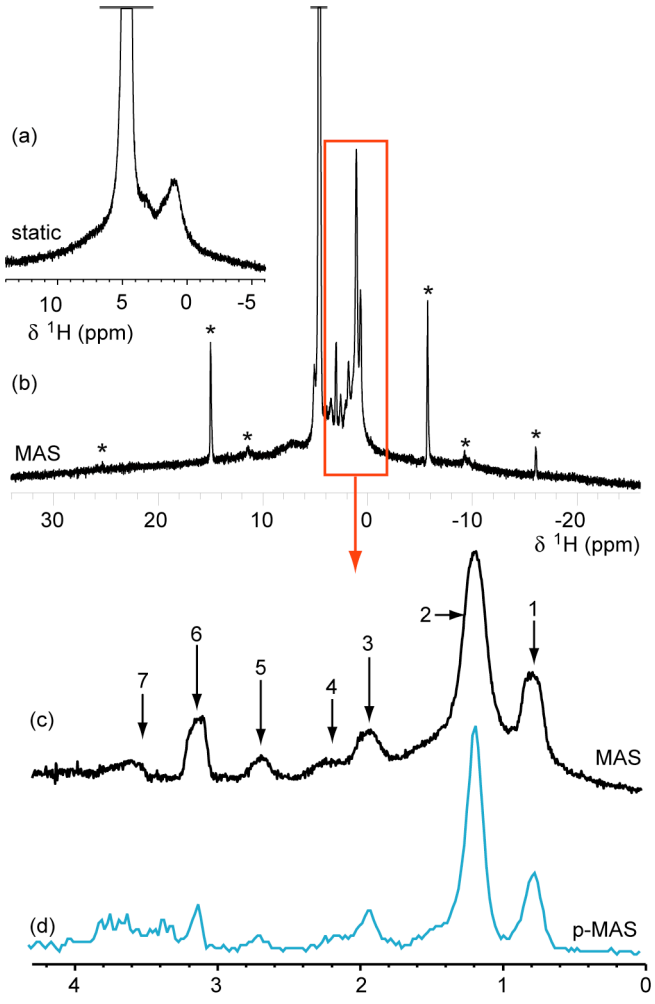
(a)
static
10
5
0
-5
δ ¹H (ppm)
(b)
MAS
*
30
20
10
0
-10
-20
δ ¹H (ppm)
(c)
MAS
7
6
5
4
3
2
1
(d)
p-MAS
4
3
2
1
0

figure 5

Figure 1: The p-MAS pulse sequence provides a method of recovering an isotropic spectrum in systems subject to anisotropic broadening without reaching the magic angle. The 2D p-MAS experiment begins with a 90° pulse, putting the magnetization into the transverse plane. It is then allowed to evolve for a period t_1 , during which the sample spins at θ_1 . Then another 90° pulse stores the magnetization along *z* in order to minimize signal decay during the rotor hopping time (τ), typically tens of milliseconds. After the hopping time τ, the magnetization is read out with a third 90° pulse and detected while spinning along θ_2 . Phase cycling is used to select the desired coherence pathway.

Figure 2: A plot of the scaling factors for the reconstructed isotropic chemical shift as a function of the two spinning angles.

Figure 3: (a) Static spectrum of bovine muscle. Resonances for water and triglyceride protons are visible, but resolution is poor. **(b)** MAS (1.7 kHz rotor frequency) spectrum of bovine muscle. Spinning sidebands of the water and trigyceride resonances are indicated with an asterisk (*). Partial assignments can be made based on literature. Peaks for individual metabolites have been identified as follows: 1. (0.8 ppm) triglyceride terminal -C**H$_3$**, or neutral amino acid -C**H$_3$**. 2. (1.2 ppm) Triglyceride –CH_2-C**H$_2$**-CH_2-, lactate, threonine -C**H$_3$** 3. (1.5 ppm) not assigned 4. (1.9 ppm) triglyceride -CH=CH-C**H$_2$**-CH_2 5. (2.1 ppm) triglyceride -CH_2-C**H$_2$**-CO 6. (4.0 ppm, 4.2 ppm) triglyceride CH=C-C**H$_2$**-CH_2, triglyceride CH_2-C**H$_2$**-CO 7. (4.7 ppm) H_2O 8. (5.2 ppm) phosphocreatine N-C**H$_3$** **(c)** Projection obtained from 2D p-MAS experiment.

Figure 4: The sequence of Fig. 1 gives a 2D spectrum in which there is a correlation between the anisotropic lineshapes given by $P_2(\cos\theta)$ at θ_1 and θ_2. Despite the broad lines in the direct and indirect dimensions, a scaled isotropic spectrum is observed along a shearing axis, the slope of which is determined by the ratio of the second Legendre polynomials for θ_1 and θ_2 This spectrum is plotted in kHz due to the chemical shift scaling. The spectrum is plotted using 20 contours following an exponential scale in order to accommodate the large range of intensities exhibited by different peaks.

Figure 5: (a) Static spectrum of bovine liver. A large water signal is observed, together with a small triglyceride resonance. **(b)** MAS (6 kHz rotor frequency) spectrum of bovine liver. Spinning sidebands of the water and trigyceride resonances are indicated with an asterisk (*). Spinning sidebands in both the muscle and liver samples were found to have on the order of 2%-5% of the centerbands, indicating that the source of broadening is uniform, consistent with the idea that it is caused by variations in the bulk susceptibility. **(c)** The region of the spectra containing the metabolite resonances is expanded. Partial assignments can be made based on literature. Peaks for tissue components have been identified as follows: 1. (0.8 ppm) triglyceride and neutral amino acid -C**H$_3$** 2. (1.2 ppm) triglyceride -CH_2-C**H$_2$**-CH_2 3. (1.9 ppm) triglyceride -CH=CH-C**H$_2$**-CH_2 4. (2.2 ppm) triglyceride -CH_2-C**H$_2$**-CO 5. (2.7 ppm) triglyceride -CH=CH-C**H$_2$**-CH=CH- 6. (3.1 ppm) choline, phosphocholine and β-glucose -C**H$_3$** 7. (3.5-3.8 ppm) glucose and glycogen 8. (4.7 ppm) water 9. (5.2 ppm) phosphocreatine N-C**H**3 **(d)** Projection obtained from 2D p-MAS experiment.